CHEMISTRY JOURNAL OF MOLDOVA. General, Industrial and Ecological Chemistry. 2025, 20(2), 72-83
ISSN (p) 1857-1727 ISSN (e) 2345-1688
http://cjm.ichem.md
https://doi.org/10.19261/cjm.2025.1367

INFLUENCE OF AROMATIC SUBSTITUENTS ON THE SYNTHESIS OF SCHIFF BASES DERIVED FROM TRANS-(*R,R*)-DIAMINOCYCLOHEXANE: A SPECTROPHOTOMETRIC AND DFT B3LYP STUDY

Lili Dahiana Becerra, Carlos Coy-Barrera*, Diego Quiroga

[a]*Bioorganic Chemistry Laboratory, Faculty of Basic and Applied Sciences, Nueva Granada Campus, Nueva Granada Military University, Cajicá 250247, Colombia*
[*]*e-mail: carlos.coy@unimilitar.edu.co*

Abstract. In this work, the synthesis of Schiff bases derived from trans-(*R,R*)-diaminocyclohexane by microwave irradiation (MW) is presented. The reaction yields varied between 31% and 69%, being influenced by the electronic nature of the substituents (H, Cl, Br, NO_2, MeO, *t*-BuO, BnO, and 4-(4-Me)PhO) and the reaction temperature. The spectrophotometric properties of the products were investigated by UV-Vis spectrophotometry, revealing bathochromic and hypsochromic effects attributable to the different substituent groups. These effects were interpreted by DFT calculations with the B3LYP functional using the 6–311G(d,p) basis set. The results suggest that the electronic properties of the substituents in the *para* position have a significant impact on the spectroscopic characteristics of the Schiff bases. The synthesized Schiff bases exhibit great potential for applications in areas such as optical sensors and functional materials, as the substituents can precisely modulate their spectrophotometric properties. This opens up new opportunities for designing compounds with tunable properties for various technological and scientific applications.

Keywords: Schiff base, MW irradiation, substituent effect, spectrophotometric property, DFT calculation.

Received: 15 September 2025/ Revised final: 28 November 2025/ Accepted: 1 December 2025

Introduction

The synthesis of trans-(*R,R*)-diamino cyclohexane-derived Schiff bases has been a topic of increasing interest due to its diverse applications in coordination chemistry and functional materials. Schiff bases have shown remarkable potential in biological applications, especially in the treatment of diabetes mellitus. Recent studies have synthesized various Schiff base derivatives with different chemical backbones, such as benzimidazole, 3,4-dihydroxyphenylacetic acid, and thiocarbazone, using multi-step methods and characterization by advanced spectroscopic techniques [1–3]. These molecules have been evaluated mainly for their inhibitory capacity of the enzymes *α*-amylase and α-glucosidase, which are key in the regulation of blood glucose levels. Several of these Schiff bases showed inhibitory activities superior to acarbose, a standard antidiabetic drug, with decreasing IC_{50} values into low micromolar range [4–6]. Molecular docking studies and dynamic simulations have allowed the characterization of the interactions with amino acid residues in the active sites of these enzymes, revealing binding mechanisms that involve hydrogen bonding, Van der Waals forces, and *π*-interactions. Furthermore, theoretical calculations based on density functional theory (DFT) and TD-DFT have provided insights into chemical reactivity, electronic stability, and properties such as electronegativity and chemical hardness, helping to explain the structure-bioactivity correlation [7,8]. Beyond their role as enzyme inhibitors, some Schiff bases, such as 2,4-dinitrophenylhydrazone derivatives, have also shown significant antioxidant potential, expanding their potential utility in modulating biological processes related to oxidative stress [9]. Together, these studies underscore the value of Schiff bases as promising multifunctional compounds for the development of novel antidiabetic and antioxidant therapies.

Recent studies (Figure 1) have explored the synthesis of N_2O_2 Schiff bases through the condensation of dehydroacetic acid with various chiral diamines, resulting in copper(II) complexes with supramolecular helical structures [10]. Furthermore, mixed Cu(II) complexes with *s*-block metals have been reported, where crystallography and mass spectrometry have enabled the analysis of their structure and reactivity [11]. Similarly, the formation of resorcinsalen-type macrocycles has

been studied to understand their supramolecular organization and their interaction with solvents [12]. On the other hand, the affinity of Ni(II) complexes with Schiff bases for quadruplex DNA structures has been investigated, demonstrating selectivity based on the chiral configuration and the presence of aromatic groups [13]. Likewise, derivatives of salen-type Schiff bases have displayed promising nonlinear optical properties due to the charge asymmetry generated by electron-donor and electron-acceptor substituents [14]. The synthesis of mononuclear copper-nickel complexes with Schiff bases has revealed their potential antimicrobial activity against bacteria such as *Staphylococcus aureus* and *Escherichia coli* [15]. The synthesis and characterization of Ni(II) and Cu(II) complexes with tetradentate Schiff base ligands have allowed the study of their stereostructural properties using vibrational circular dichroism (VCD) spectroscopy, UV-Vis spectroscopy, and electron circular dichroism (ECD), highlighting the conformational sensitivity of the ligands and the induced helicity in the metal complexes [16]. Similarly, studies with Fe(II) complexes have demonstrated meridional configurations and hydrogen-bonding interaction networks in their crystal structures [17]. The self-assembly of supramolecular structures from chiral diamines has also been of interest, where the modulation of intramolecular forces has allowed the synthesis of unusual quadrangular tubes stabilized by C−H···π interactions [18]. Some reports in the literature have not only informed about the synthesis and characterization of Schiff bases but also their metal complexes, highlighting their potential in catalysis and supramolecular chemistry [19–21].

These structural and supramolecular characteristics have allowed direct, specific applications of this family of compounds. The fabrication of a chiral stationary phase (CSP) based on a homochiral [4+6] porous organic cage (POC) CC19-R, covalently bonded to thiolated silica *via* a thiol-ene click reaction, has been reported. This stationary phase demonstrated superior enantioselective separation capacity in normal and reversed-phase HPLC, efficiently separating chiral compounds such as 4-chlorobenzhydrol and cetirizine dihydrochloride, with resolutions up to 6.50 [22]. Comparisons with commercial columns such as Chiralpak AD-H and Chiralcel OD-H highlighted their complementarity and effectiveness in separating certain racemates. Furthermore, novel Schiff bases derived from trans-1,2-diaminocyclohexane have demonstrated selective sensitivity toward Cr(III) and Cu(II) through hydrolytic cleavage mechanisms of C=N bonds, opening new possibilities for detecting toxic ionic species in water [23].

These potential applications have drawn the attention of several researchers seeking alternatives that could enhance the existing synthetic protocols based on the Schiff reaction. Microwave (MW) irradiation has proven to be a highly efficient, rapid, and environmentally friendly tool for the synthesis of Schiff bases, with a significant impact on both product yield and functional properties [24]. The synthesis of chitosan-derived Schiff bases under MW irradiation yielded compounds with high corrosion inhibition efficiency (up to 90.65% at 50 ppm), using a cleaner and faster methodology compared to conventional methods, which utilize controlled temperature and power conditions to facilitate the reaction [25]. Similarly, other studies have reported that this approach dramatically shortens reaction times (from 6–8 hours to just minutes) and improves product yields and purity, as in the case of isoniazid Schiff bases [26]. Furthermore, MW-catalysed reactions with cashew nutshell extract showed that even under solvent-free conditions, Schiff base-type products were obtained in reduced times and with yields exceeding 88% [27]. MW-assisted synthesis is not only energy-efficient but also promotes greener and more sustainable conditions, reducing the need for toxic solvents or additional reagents while enabling the exploration of new applications, such as antimicrobial dyes in textiles [28]. This evidence underscores the growing significance of this technique in green chemistry and the rational design of functional compounds, such as Schiff bases.

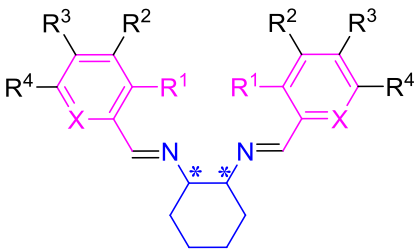

R^1 = OH; R^2 = R^3 = R^4 = H; X = CH [1]
R^1 = OH; R^2 = OEt; R^3 = R^4 = H; X = CH [2]
R^1 = OH; R^2 = R^3 = H; R^4 = NO_2; D, X = CH [5]
R^1 = OH; R^2 = R^4 = H; R^3 = Br, F; X = CH [6]
R^1 = OH; R^2 = R^4 = *t*-Bu; R^3 = H; X = CH [7]
R^1 = R^2 = R^3 = R^4 = H; X = N [8]

Figure 1. Representative structure of Schiff bases derived from trans-1,2-diaminocyclohexane.

This study demonstrates the efficient microwave-assisted synthesis of Schiff bases **1**–**8**, revealing how the electronic and steric effects of *para*-substituents on the benzene ring significantly influence yields and physicochemical properties. Electronegative groups enhance reactivity by activating the carbonyl carbon, while electron-donating groups reduce reactivity and introduce steric hindrance. Reaction temperature critically affects yield, with excessive heat causing product decomposition. Structural confirmation *via* ATR-FTIR, NMR, HRMS, and DFT calculations showed that substituent electronics impact chemical shifts and optical properties, including UV-Vis absorption and the HOMO-LUMO gap. Using benzaldehydes with diverse substituents (R= H, Cl, Br, NO_2, MeO, *t*-BuO, BnO, 4-(4-Me)PhO), were correlated yields and photophysical behaviour to electronic effects, supported by DFT at the B3LYP at the level 6-311G(d,p) level. UV-Vis spectroscopy revealed bathochromic and hypsochromic shifts linked to substituent nature, providing insights for the rational design of Schiff bases with tunable optical properties. These findings advance the development of materials and catalysts, particularly for transition metal complexes with desirable photochemical features [29–31].

Experimental

Generalities

All chemicals were purchased from Sigma-Aldrich (Saint Louis, MO, USA) and Merck KGaA (Darmstadt, Germany) and used without further purification. Dry solvents were purchased at appropriate purity. Thin-layer chromatography (TLC) was performed on silica gel 60 F254 (Merck KGaA), and compounds were detected at 254 nm. Column chromatography was performed manually using silica gel 60 (0.040–0.063 mm) from Merck KGaA. Nuclear magnetic resonance (NMR) spectra were recorded on a Bruker Avance AV-400 MHz spectrometer (Billerica, MA, USA). All shifts are expressed in δ (ppm) using the tetramethylsilane (TMS) signal as a reference. Coupling constants (*J*) are given in Hz. Splitting patterns are typically described as follows: *s*: singlet, *d*: doublet, *t*: triplet, *q*: quartet, and *m*: multiplet. FT-IR spectra were measured on a Jasco FT/IR-6600typeA spectrophotometer (JASCO Co., Ltd., Mary's Court, PA, USA) coupled to an ATR PRO ONE accessory with an incidence angle of 45 degrees and a resolution of 4 cm^{-1}. High-resolution Mass spectrometry was performed on a UHPLC Shimadzu Nexera X2 chromatograph coupled to a QTOF LCMS-9030 spectrometer. Formic acid 0.1%: methanol 40:60 was employed as the mobile phase, with a total run time of 20 min, using a Shim-pack HR-ODS column 150 mm L × 3 mm ID, 80 A°. The analysis was performed in both positive and negative ion modes, with the most suitable mode being ESI+. The chemical reactions were carried out in a Single-mode Discover System MW reactor model 908,005 series DY1030 in the open vessel method, with the temperature controlled at 80°C, an internal pressure between 0 and 10 psi, and MW power of 200 W. For the UV-Vis spectra measurement, GENESYS 10S UV-Vis spectrophotometer (v4.005, serial number 2L5S125220) was used. The analysis was performed in Absorbance mode, with a spectral scan ranging from 190.0 nm to 800.0 nm at an interval of 1.0 nm.

Synthesis of Schiff Bases

The synthesis of Schiff bases was performed by reacting trans-(*R*,*R*)-diaminocyclohexane L(+)-tartrate (1 mmol) with the corresponding *p*-substituted benzaldehyde (2 mmol) under microwave irradiation in open-vessel mode. The reaction mixture was heated at 80°C for 40 minutes. The progress of the reaction was monitored by thin-layer chromatography (TLC) using silica gel plates, with varying ratios of hexane and ethyl acetate as the mobile phase. Upon completion, the crude product was purified by column chromatography employing silica gel as the stationary phase and a hexane: ethyl acetate mixture as the eluent to afford the desired Schiff base in pure form. Characterization data of compounds **1-5** are consistent with those reported previously in literature [32-36].

(1*E*,1'*E*)-*N*,*N*'-((1*R*,2*R*)-cyclohexane-1,2-diyl)*bis*(1-(4-(benzyloxy)phenyl)methanimine) **6**. Yellow wax. IR (neat, ATR, cm^{-1}): 3031, 2922, 2856, 1599, 1508, 1238, 735. ^{1}H NMR (400 MHz, $CDCl_3$) δ 8.15 (*s*, 1H), 7.56 (*d*, *J*= 8.8 Hz, 4H), 7.52–7.49 (*m*, 6H), 7.00 (*d*, *J*= 8.7 Hz, 4H), 6.91 (*d*, *J*= 8.8 Hz, 4H), 5.02 (*s*, 4H), 3.40 (*m*, 2H), 1.98–1.77 (*m*, 6H), 1.51 (*m*, 2H). ^{13}C NMR (101 MHz, $CDCl_3$) 160.8, 160.4, 143.1, 136.6, 130.0, 128.6, 125.1, 115.3, 114.7, 73.8, 70.0, 33.1, 27.4. ESI+-HRMS m/z $[M+H]^+$, 503.2690 (calcd. 503.2693, $C_{34}H_{34}N_2O_2$). R_f in hexane: ethyl acetate (8:2): 0.88.

(1*E*,1'*E*)-*N*,*N*'-((1*R*,2*R*)-cyclohexane-1,2-diyl)*bis*(1-(4-(*tert*-butoxy)phenyl)methanimine) **7**. Orange wax. IR (neat, ATR, cm^{-1}): 3058, 2926, 2856, 1634, 1597, 1498, 1236, 893. ^{1}H NMR (400 MHz, $CDCl_3$) δ 8.16 (*s*, 2H), 7.51 (*d*, *J*= 8.6 Hz, 4H), 6.93 (*d*, *J*= 8.6 Hz, 4H), 3.47–3.24 (*m*, 2H), 1.89–1.70 (*m*, 6H), 1.53–1.44

(*m*, 2H), 1.34 (*s*, 18H). ^{13}C NMR (101 MHz, $CDCl_3$) δ 160.6, 157.6, 131.6, 128.8, 123.6, 79.0, 73.8, 33.1, 29.0, 24.6. ESI+-HRMS m/z $[M+H]^+$, 435.3041 (calcd. 435.3006, $C_{28}H_{38}N_2O_2$). R_f in hexane: ethyl acetate (8:2): 0.82.

(1*E*,1'*E*)-*N*,*N*'-((1*R*,2*R*)-cyclohexane-1,2-diyl)*bis*(1-(4-(*p*-tolyloxy)phenyl)methanimine) **8**. Yellow wax. IR (neat, ATR, cm^{-1}): 3028, 2921, 2854, 1640, 1597, 1496, 1232, 812. ^{1}H NMR (400 MHz, $CDCl_3$) δ 8.17 (*s*, 2H), 7.57 (*d*, *J*= 8.7 Hz, 4H), 7.14 (*d*, *J*= 8.1 Hz, 4H), 6.92–6.89 (*m*, 8H), 3.42–3.37 (*m*, 2H), 2.34 (*s*, 6H), 1.97–1.77 (*m*, 6H), 1.55–1.43 (*m*, 2H). ^{13}C NMR (101 MHz, $CDCl_3$) 160.0, 159.9, 154.0, 142.8, 133.7, 130.3, 125.8, 119.8, 117.8, 73.9, 33.1, 27.5, 20.8. ESI+-HRMS m/z $[M+H]^+$, 503.2690 (calc. 503.2693, $C_{34}H_{34}N_2O_2$). R_f in hexane: ethyl acetate (8:2): 0.87.

UV-Vis spectrum measurement

The Schiff bases **1-8** UV-Vis spectra were measured using a spectrophotometer with a wavelength range of 190 nm to 800 nm. Quartz cuvettes with a standard capacity of 5 mL were used for measurements, which do not absorb in the UV-Vis. The Schiff base was dissolved in dichloromethane (2.0 mM), and the solution cell was introduced into the spectrophotometer. The absorption spectrum was recorded from 190 nm to 800 nm, covering both the ultraviolet (UV) and visible regions. The characteristic absorption bands were identified primarily in the 250 nm to 450 nm range for both C=C and C=N π-π* transitions.

Computational calculations

Computational calculations were performed using the Spartan'18 PC software package. The initial molecular geometries of compounds **1-8** were constructed based on experimental data and literature precedents when available, or built de novo using the molecular builder tool within Spartan. All geometries were fully optimized without imposing any symmetry constraints to allow for unbiased conformational relaxation. Geometry optimizations were carried out using Density Functional Theory (DFT) with the hybrid Becke three-parameter exchange functional combined with the Lee-Yang-Parr correlation functional (B3LYP), known for its reliable balance between accuracy and computational cost. The 6-311G(d,p) triple-zeta basis set, which includes polarization functions on both heavy atoms and hydrogens, was employed to provide a flexible and accurate description of the electronic environment. All stationary points were confirmed as minima by vibrational frequency analysis, performed at the same level of theory (B3LYP using 6-311G(d,p) basis set), ensuring the absence of imaginary frequencies. Thermal corrections to Gibbs free energies and enthalpies were calculated from frequency data at 298 K and 1 atm, following the harmonic oscillator and rigid rotor approximations. Molecular orbital analyses, including HOMO-LUMO gap calculations and natural bond orbital (NBO) analysis, were performed to gain insight into electronic properties. Visualization of molecular orbitals and electrostatic potential maps was conducted using the Spartan graphical interface.

Results and discussion

Schiff bases **1-8** were synthesized using a MW-assisted protocol using trans-(*R*,*R*)-diamino cyclohexane and benzaldehydes (Scheme 1). The yields for synthesizing these compounds (Table 1) revealed an interesting dependence on both the electronic and steric nature of the substituents on the benzaldehydes and the reaction temperature. These aspects are discussed below. *Para*-position substituents significantly affect the reactivity in the formation of Schiff bases **1-8**. Electron-withdrawing groups (EWGs), such as halogens and nitro groups, can decrease the electron density of the aromatic ring, making it more electrophilic and favouring the condensation reaction with trans-(*R*,*R*)-diaminocyclohexane. Electron-donating groups (EDGs), such as methoxy (MeO) and benzyloxy (BnO), increase the electron density of the aromatic ring, disfavouring the Schiff reaction.

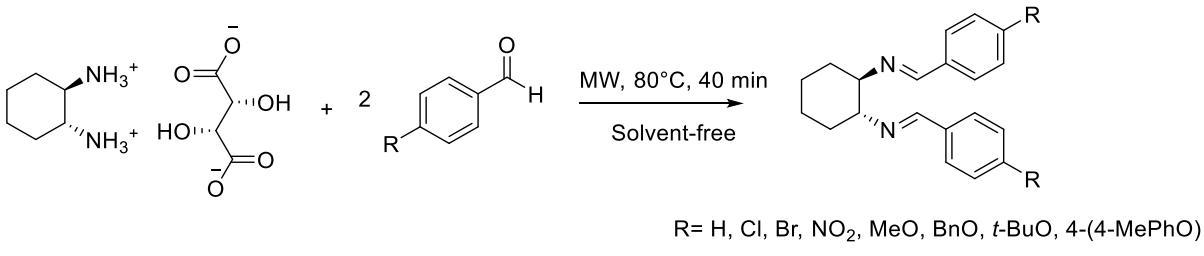

R= H, Cl, Br, NO_2, MeO, BnO, *t*-BuO, 4-(4-MePhO)

1-8

Scheme 1. Synthesis of Schiff bases 1-8.

Using benzaldehydes with electron-withdrawing groups (EWGs) (Cl, Br, NO_2) showed increasing yields, depending on the reaction temperature, suggesting greater molecular mobility and overcoming the energy barriers associated with Schiff base formation, mainly related to the favoured loss of water molecules [37]. EDGs such as MeO, BnO, and *t*-BuO showed moderate yields compared to EWGs, especially at lower temperatures. In addition to electronic effects, the results suggested that *para*-position substituents can induce steric effects that influence the accessibility of amine groups in benzaldehydes and, consequently, their reactivity [38]. In this case, bulkier substituents, such as the *t*-butoxy group (*t*-BuO) and the 4-(4-methylphenoxy) group (4-(4-Me)PhO), could induce additional steric hindrance. At higher temperatures (80°C and 120°C), the steric effects of bulkier groups, such as *t*-BuO and 4-(4-methylphenoxy), are less significant due to greater thermal agitation, allowing the reaction to proceed more easily [39]. Regarding the influence of temperature, yields typically increase with rising temperatures. This is consistent with the expected behaviour for a Schiff reaction, where higher temperatures favour reaction kinetics by providing more energy to overcome activation barriers [40].

However, there is a tendency for yields to plateau or slightly decrease at very high temperatures (120°C), which may be related to the partial decomposition of the products or the formation of side products due to thermal overload [41]. Interestingly, some of the lowest yields are obtained at 40°C, suggesting that the formation of Schiff bases is more difficult under these conditions. This is likely due to a slower reaction rate, especially for substituents that do not electronically favour the reaction, such as the nitro group. A comparison has been made between a previously published protocol and our results. The synthetic protocol reported by Cívicos, J *et al*. is based on manual grinding of reagents, which allows for the obtaining of Salen-type Schiff bases in excellent yields (up to 95%) after 10 to 20 minutes of grinding at a 0.5–2.0 mmol scale, without the need for additional heating [35]. In contrast, the proposed method utilizes MW irradiation, achieving reaction completion in 40 minutes at controlled temperatures ranging from 40 to 120°C. Although the use of MWs facilitates thermal control and can favour reactions with less reactive benzaldehydes, the yields obtained in the MW-assisted protocol are generally lower than those reported by Cívicos, J. *et al*., especially for simple derivatives such as compound **1**, where a 39% maximum yield was obtained compared to the 55% reported in the literature. These low yields for compounds **1-5** could be attributed to the effect of prolonged MW irradiation on Schiff bases. It has been shown that these compounds undergo decomposition when heated in the presence of air [42-45]. Some reports have shown that the presence of a nitro group can favour their thermal stability up to approximately 160°C. However, decomposition can extend up to 310°C, with endothermic effects associated with melting and exothermic effects due to molecular destruction. The presence of oxygenated groups, which confer greater thermal stability up to 204°C, results in a two-stage degradation process between 204 and 357°C, as evidenced by both endothermic and exothermic effects. The electronic nature of the groups explains these stabilization effects. The nitro group exerts an electron-withdrawing mesomeric effect, which stabilizes the structure, while the hydroxyl group has a donating mesomeric effect [42]. However, since MW irradiation causes *hot spots* that can easily exceed the temperature of the reaction mixture, reaching 200°C or more, these local conditions could induce the reactivity of Schiff bases **1-8** until their degradation.

Table 1

Yields for the synthesis of Schiff bases 1-8 at different temperatures.

		T = 40°C	*T= 80°C*	*T= 120°C*	
Compound	*R*	*% Yield*	*% Yield*	*%Yield*	*% Yield [reference]*
1	H	31	39	32	55 [23]
2	Cl	37	69	62	95 [24]
3	Br	39	67	61	91 [25]
4	NO_2	38	65	55	65 [26]
5	MeO	36	68	52	44 [27]
6	BnO	38	66	59	No reported
7	*t*-BuO	39	69	52	No reported
8	4-(4-MePhO)	35	62	57	No reported

Nevertheless, the MW-assisted protocol can be used effectively for benzaldehydes with bulky and π-extended aromatic groups, such as the employed precursors for the synthesis of compounds **6**–**8**. These results are attributed to the reactivity of these *para*-substituted benzaldehydes as electrophiles with BnO (benzyloxy), *t*-BuO (*tert*-butyloxy), and 4-(4-MePhO) groups, which varies according to the electronic effects they exert on the carbonyl group. The BnO and 4-(4-MePhO) groups are resonance donors because they possess an extended π-aromatic system, which reduces the electrophilicity of the carbonyl; this effect is more substantial in the latter due to the extended resonance of the methoxy group. The *t*-BuO group primarily acts through an inductive effect, albeit in a weaker manner, resulting in a slight decrease in reactivity. Thus, the MW-assisted protocol also offers several advantages, including greater reproducibility for a broad range of precursors, the possibility of scaling up reactions, and the avoidance of using organic solvents during synthesis.

The structural elucidation of the synthesized Schiff bases **1**–**8** was carried out using spectroscopic techniques such as Attenuated total reflectance Fourier transform infrared spectroscopy (ATR-FTIR), high-resolution mass spectrometry (HRMS), and ^{1}H and ^{13}C NMR nuclear magnetic resonance spectroscopy. The results showed that the electronic effects of the substituents significantly impact the chemical shifts observed in both the protons and carbons of the system. The ATR-FT-IR spectra of Schiff bases **1**–**8** (Figure S1–S8, supplementary information) showed characteristic absorption bands that correspond to the functional groups present in these compounds, identifying structural moieties such as the C–N, C=C, C=N, and C–H bonds through the assignment of the respective stretching vibrations (Table 2). The C-N band stretching bands were detected between 1093 and 1196 cm^{-1}, consistent with the literature [46] (1093–1195 cm^{-1}). The position of the stretching band varies depending on the substituent on the benzene ring, indicating that the electronic effects introduced by the substituents affect the vibration frequency of the C-N bond. Compounds with electron-withdrawing groups (EWGs), such as Cl (**2**, 1093 cm^{-1}) and NO_2 (**4**, 1196 cm^{-1}), exhibited a slight shift in band position, consistent with the effect of reducing electron density on nitrogen, potentially increasing the C–N bond vibration frequency. The C=C bond-stretching bands were between 1449 cm^{-1} and 1519 cm^{-1} (literature: 1419–1595 cm^{-1}). Compounds with larger or EWGs substituents, such as NO_2 (**4**, 1519 cm^{-1}) and BnO (**7**, 1499 cm^{-1}), showed shifts toward higher values, which may be related to the greater rigidity or conjugation effects of the substituents. This behaviour is consistent with the fact that larger or more resonant groups can alter the vibrational characteristics of the C=C double bond. The C=N bond-stretching bands appeared in the range of 1597 cm^{-1} to 1630 cm^{-1}. The wavenumber of these bands is quite consistent with the values reported in the literature (1597–1627 cm^{-1}), indicating that the Schiff base structure is maintained despite the different substituents on the benzene ring. However, compounds such as **3** (Br, 1630 cm^{-1}) observe a slight shift toward higher frequencies. The C-H stretching of the imine group is observed around 3070–3107 cm^{-1}, within the range reported in the literature (3075–3140 cm^{-1}). This band does not show significant variations between compounds **1**–**8**.

The results of the ATR-FT-IR spectra show a clear dependence of the position of the absorption bands on the substituents on the benzene ring. Electronegative groups such as Cl and NO_2 influence the frequencies of C–N, C=C, and C=N stretching, shifting them slightly toward higher values, which can be attributed to inductive and resonance effects.

Table 2

Representative ATR-FT-IR absorption bands for compounds 1-8.

Compound	*R*	*ν C-N stretching / cm^{-1}*		*υ C=C stretching / cm^{-1}*		*υ C=N stretching / cm^{-1}*	
		Experimental	*Calculated*	*Experimental*	*Calculated*	*Experimental*	*Calculated*
1	H	1117	1088	1449	1418	1600	1626
2	Cl	1093	1098	1487	1420	1593	1639
3	Br	1168	1095	1484	1427	1630	1641
4	NO_2	1196	1121	1519	1429	1598	1595
5	MeO	1160	1191	1509	1434	1604	1552
6	BnO	1171	1201	1499	1452	1599	1557
7	*t*-BuO	1149	1156	1498	1461	1597	1548
8	4-(4-MePhO)	1159	1121	1496	1429	1597	1595

To correctly assign these described vibration bands, DFT computational calculations using the B3LYP method were performed. Although the calculated values agree with the experimental values, some discrepancies were detected, which can be attributed to the inherent limitations of the computational methods and the experimental conditions. In general, the calculated values tend to underestimate the C–N and C=C stretching frequencies, while for the C=N bond, they are slightly overestimated in most cases. These discrepancies may be because calculations are typically performed in the gas phase and under ideal conditions. Experimental spectra are usually obtained in the solid state or in solution, where intermolecular interactions and environmental effects can significantly influence molecular vibrations. Nevertheless, these calculations helped complement the characterization of compounds **1**–**8**.

HRMS spectra (Figure S11, S14, S17, supplementary information) confirmed the proposed structure for compounds **1**–**8**. For compounds **6** and **8**, the exact calculated mass of the $[M+H]^+$ ion correlated with the experimental mass. The deviation observed in both cases was lower than 0.596 ppm, indicating excellent agreement between the theoretical and experimental values. Compound **7** showed a discrepancy between the calculated and experimental values. The exact theoretical mass was 435.3006, while the experimentally obtained mass was 435.3041, with an error of 8.04 ppm.

Analysis of the ^{1}H NMR spectra (Figure S9, S12, S15, supplementary information) demonstrated that the substituent group in the *para* position primarily affects the magnetic environment of the protons in the aromatic ring and the cyclohexane system, depending on the electronic nature of the substituents. For compound **6** (R= BnO), the proton shifts of the cyclohexane system are typical, with signals at 1.51 and 1.87 ppm for the methylene hydrogens and 3.35 ppm for the methylene hydrogens. The imine hydrogen is observed at 8.15 ppm, which is characteristic of this type of imine bond. The presence of a signal pattern in the range of 6.91–7.43 ppm for the aromatic protons, with typical couplings, suggests that the benzyl group does not generate a very strong electronic effect but does cause a slight interaction with the aromatic ring. This behaviour is consistent with the slight electron-donating effect of the benzyl group, which can slightly depolarise the imine ring, causing small changes in the shifts. For compound **7** (R= *t*-BuO), similar shifts are observed for the cyclohexane hydrogens as in the base with compound **6**, but with a slight change in the shifts of the aromatic protons, which are found at 6.93 and 7.51 ppm. This result suggests that the *t*-BuO group, being a more substantial electron donor than the benzyl group, causes a slight increase in the electron density of the aromatic ring. This higher electron density may facilitate electron donation to the imine system, causing a subtle change in the shifts of the aromatic protons. For compound **8**, where the substituent is the 4-methylphenoxy group, an electron donor effect was observed, which is reflected in the shifts of the aromatic protons in the range of 6.95–7.53 ppm. Furthermore, the slight alteration observed in the shifts of the cyclohexane system can be attributed to the electronically inductive interaction of oxygen with the phenoxy group. This substituent appears to have a moderate effect on modifying the electron density of the aromatic ring, slightly altering the proton shifts. With typical couplings, EWGs such as the NO_2 group (compound **4**) result in shifts of the aromatic protons at 7.29 and 7.60 ppm. This group decreases the electron density in the aromatic ring, resulting in higher shifts than electron-donating substituents. This result highlights the significant influence of electron-withdrawing groups on the electronic structure of Schiff bases.

The chemical shifts of the carbon atoms, obtained from the ^{13}C NMR spectra (Figure S10, S13, S16, supplementary information), exhibited patterns like those observed in the ^{1}H NMR spectra. For compound **6**, a shift is observed at the imine carbon at 160.7 ppm and an additional shift at the aromatic carbon atoms at 160.2 ppm. In the case of the compound **7** (R= *t*-BuO), the carbon shifts are like those observed for **6**. Still, the aromatic carbon atoms showed an additional shift at 157.7 ppm, indicating an increase in electron density in the aromatic ring due to the electron-donating effect of the *t*-BuO group. For compound **4** (containing a NO_2 group), the shifts of the aromatic carbon atoms are in the range of 115–140 ppm, with an additional shift at 154.0 ppm. This result confirmed that the NO_2 group acts as a strong electron-withdrawing group (EWG), decreasing the electron density in the aromatic ring, which is reflected in the shifts to lower values.

UV-Vis absorption spectra of Schiff bases **1-8** (Figure 3) revealed the impact of the substituent (R) on electronic transitions, influencing both the wavelengths of maximum absorption (λ_{max}) and the molar absorptivity coefficients (ε), which were established using the

first derivative criterion [47] (Table 3). Furthermore, B3LYP DFT calculations at the level 6-311G(d,p) allowed these spectroscopic effects to be correlated with the energies of the frontier orbitals (HOMO and LUMO) and the HOMO-LUMO gap. The relationship between the electronic effects of substituents and the photophysical properties of organic compounds has been extensively studied using density functional theory (DFT) and its extensions, such as time-dependent DFT (TDDFT). These studies have shown that the electronic nature of substituents significantly influences electronic transitions, excitation energy, and emission quantum efficiency. For example, in 2-(2-hydroxyphenyl)benzothiazole (HBT) derivatives, substituents such as -CN, -CO_2Me, and -Cl were observed to favour intramolecular proton transfer processes in the excited state, while groups such as -NO_2 inhibit them. These effects correlate with the electron density in the active regions of the molecule, determined by DFT calculations [47]. Furthermore, Hammett theory has been applied to quantify how electron-donating or electron-withdrawing substituents affectthe optical properties of systems such as diketopyrrolopyrrole (DPP) derivatives. DFT and TDDFT calculations have shown that the introduction of electron-donating groups reduces the HOMO-LUMO gap and shifts the maximum absorption wavelengths, whereas electron-withdrawing groups have the opposite effect [48]. In compounds such as fluorescent phenylhydrazones, the core molecular structure has been observed to be the main determinant of the emission properties, while the effects of the substituents are more evident in the fluorescence intensity and quantum yields. DFT calculations have been essential for interpreting these behaviours, providing information on the electron distribution and molecular interactions [49]. These results allowed us to establish that the EDG or EWG nature of the substituent directly influences the shift in λ_{max}. It is observed that compound **4** with a NO_2 group exhibited the most marked red shifts (bathochromic effect), with values of 344 nm and 410 nm [37]. This effect can be attributed to its strong electron-withdrawing nature, which stabilizes the excited state and lowers the energetic transition.

Table 3

Representative results from UV-Vis spectra analysis for compounds 1-8.

Compound	*R*	λ_{max} *1 /nm*	ε */ M^{-1} cm^{-1}*	λ_{max} *2 /nm*	ε */ M^{-1} cm^{-1}*	*Gap HOMO-LUMO / eV*
1	H	264	176	334	40	5.06
2	Cl	247	133	315	26	4.92
3	Br	253	185	313	5	4.88
4	NO_2	346	40	404	15	4.21
5	MeO	264	148	322	11	4.84
6	BnO	263	144	318	134	4.83
7	*t*-BuO	258	200	322	7	4.71
8	4-(4-MePhO)	268	80	314	80	4.8

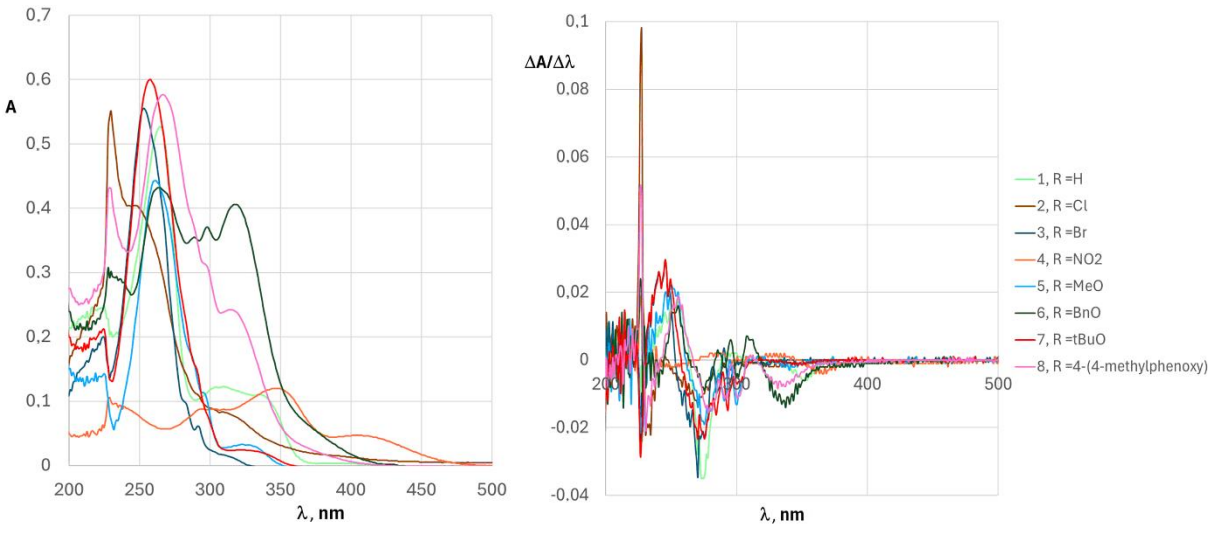

(a) ***(b)***

Figure 3. UV-Vis analysis of compounds 1–8: UV-Vis spectra *(a)*; First derivative of UV-Vis spectra *(b)*.

In contrast, compounds with halogen substituents (Cl and Br), such as **2** and **3**, exhibit shorter wavelengths (251–253 nm and 313–315 nm), indicating a relative hypsochromic effect due to their lower ability to stabilize the excited state compared to the NO_2 group. Electron-donating substituents, such as methoxy (MeO), *tert*-butyloxy (*t*-BuO) and benzoyloxy (BnO) groups, also produce bathochromic shifts relative to the unsubstituted compound **1**, although to a lesser extent than NO_2. This suggests that donating electron density to the conjugated system stabilizes the excited state, reducing the energy of the electronic transition. The molar absorptivity coefficient (ε) reflects the intensity of the electronic transitions. A significant hyperchromic effect is observed in the compound with a *t*-BuO group (ε= 200 M^{-1} cm^{-1} at 258 nm), indicating a higher transition probability due to the increased electron density in the conjugated system. In contrast, compound **4** (with a NO_2 group) showed significantly lower ε values (40 M^{-1} cm^{-1} at 344 nm and 15 M^{-1} cm^{-1} at 410 nm), reflecting a hypochromic effect that could be attributed to a decrease in the overlap of the molecular orbitals involved in the transition. The HOMO-LUMO gap reveals how the substituent's electronic nature modulates the stability of the frontier orbitals. Compound **4** has the smallest bandgap (4.21 eV), indicating greater ease of electronic excitation and justifying the bathochromic shift observed in the UV-Vis spectrum. In contrast, the compound **1** without a substituent has a band gap of 5.06 eV, the largest in the series, consistent with its lower λ_{max}. Compounds with electron-donating substituents (MeO, BnO, *t*-BuO) also exhibit smaller band gaps (4.84–4.71 eV), suggesting that these groups facilitate the electronic transition by stabilizing the excited state. In contrast, halogenated compounds **2-3** (Cl and Br) have intermediate band gap values (4.92 and 4.88 eV, respectively), suggesting that their effect is moderate compared to the other substituents. It is relevant to specify that although the calculated HOMO-LUMO gap can be related to the electronic transition energy observed in UV-Vis spectroscopy, where a smaller gap typically corresponds to absorptions at longer wavelengths due to greater electron delocalization and conjugation in the molecule, the HOMO-LUMO gap obtained by DFT represents the fundamental gap. In contrast, the UV-Vis absorption measures the optical gap, which includes exciton effects and electronic relaxation, which can generate some discrepancies between calculations and experiments.

These results reveal that the electronic nature of the substituent has a significant influence on the spectroscopic shift of Schiff bases at the *para* position of the benzene ring. Electron-donating groups induce bathochromic and, in some cases, hyperchromic effects, while electron-withdrawing groups, such as nitro, cause the most pronounced bathochromic shifts and hypochromic effects. Correlation with DFT calculations supports these observations, indicating that the decrease in the HOMO-LUMO gap is directly related to the λ_{max} shift and the ease of electronic transition.

These results significantly advance previous studies by providing a comprehensive analysis of the combined effect of the electronic and steric nature of the substituents in benzaldehydes on the synthesis and properties of Schiff bases. Unlike previous reported protocols, the microwave-assisted methodology reported here offers precise thermal control, allowing us to observe how both electron-donating and electron-withdrawing groups affect the yields and thermal stability of the products, providing novel insights into the influence of temperature in overcoming energy barriers and minimizing steric effects. Furthermore, spectroscopic characterization combined with DFT calculations allows us to correlate the electronic effects of the substituents with structural and photophysical changes, revealing how these modify electron density, molecular vibration, and the HOMO-LUMO gap-key information for the rational design of optical materials with tunable properties. Thus, this research integrates synthesis, characterization, and theoretical modeling to deepen the understanding of the chemistry and electronic properties of Schiff bases beyond previous studies, laying the groundwork for future functional applications.

Conclusions

Microwave-assisted synthesis of Schiff bases **1**–**8** showed an evident influence of the electronic and steric properties of the substituents on product yield and stability. Electronegative groups increase reactivity and favour higher yields, while electron donors and bulky substituents decrease efficiency, especially at low temperatures. Spectroscopic characterization and DFT calculations confirmed that these effects modify electron density, molecular vibrations, and the HOMO-LUMO gap, thus affecting the optical properties of the Schiff bases. The MW-assisted protocol offers advantages in reproducibility, thermal control, scalability, and solvent-free

synthesis, being especially suitable for derivatives with bulky substituents or extended aromatic systems. However, it is limited by lower yields for simple derivatives, likely due to thermal decomposition induced by prolonged irradiation. These findings provide a comprehensive understanding of the structure-property relationship and lay a solid foundation for the rational design of functional optical materials.

Acknowledgments

The present work is derived from the project INV-CIAS 3953 financed by Universidad Militar Nueva Granada–Validity 2024.

Supplementary information

Supplementary data are available free of charge at http://cjm.ichem.md as PDF file.

References

1. Fonkui, T.Y.; Ikhile, M.I.; Njobeh, P.B.; Ndinteh, D.T. Benzimidazole schiff base derivatives: synthesis, characterization and antimicrobial activity. BMC Chemistry, 2019, 13(1), pp. 127–138. DOI: https://doi.org/10.1186/s13065-019-0642-3
2. Alam, A.; Badshah, G.; Ayaz, M.; Zainab; Elhenawy, A.A.; Ahmad, I.; Shah, S.A.A.; Latif, A.; Ali, L.; Ali, M.; Ahmad, M. Bis-Schiff bases as potent antidiabetic agents: synthesis, enzyme inhibition, molecular docking and dynamic simulations. Journal of Molecular Structure, 2026, 1351(1), pp. 144173–144188. DOI: https://doi.org/10.1016/j.molstruc.2025.144173
3. Jan, F.; Idris, S.; Waheed, M.; Alam, A.; AlAsmari, A.F.; Alasmari, F.; Khan, M. Thiosemicarbazone derivatives as potent antidiabetic agents: synthesis, *in vitro*, molecular docking and DFT investigations. Journal of Molecular Structure, 2024, 1311, 138459, pp. 1–15. DOI: https://doi.org/10.1016/j.molstruc.2024.138459
4. Shakoor, A.; Fareed, G.; Ahmad, I.; Elhenawy, A.A.; Khan, M.; Fareed, N.; Al-Olayan, E.; Abukhadra, M.R.; Alam, A.; Ibrahim, M. Exploring the anti-diabetic activity of benzimidazole containing Schiff base derivatives: *in vitro* *α*-amylase, α-glucosidase inhibitions and *in silico* studies. Journal of Molecular Structure, 2025, 1321(5), pp. 140136–140151. DOI: https://doi.org/10.1016/j.molstruc.2024.140136
5. Khan, M.; Gohar, H.; Alam, A.; Wadood, A.; Shareef, A.; Ali, M.; Khalid, A.; Abdalla, A.N.; Ullah, F. Para-substituted trhiosemicarbazones as cholinesterase inhibitors: synthesis, *in vitro* biological evaluation, and *in silico* study. ACS Omega, 2023, 8(5), pp. 5116–5123. DOI: https://doi.org/10.1021/acsomega.2c08108
6. Khan, H.; Jan, F.; Shakoor, A.; Khan, A.; AlAsmari, A.F.; Alasmari, F.; Ullah, S.; Al-Harrasi, A.; Khan, M.; Ali, S. Design, synthesis, molecular docking study, and α-glucosidase inhibitory evaluation of novel hydrazide–hydrazone derivatives of 3,4-dihydroxyphenylacetic acid. Scientific Reports, 2024, 14(1), pp. 11410–14419. DOI: https://doi.org/10.1038/s41598-024-62034-x
7. Babaei, P.; Hadigheh-Rezvan, V.; Sohrabi-Gilani, N.; Rostamzadeh-Mansour, S. Molecular docking and *in vitro* biological studies of a Schiff base ligand as anticancer and antibacterial agents. Results in Chemistry, 2024, 7, pp. 101517–101531. DOI: https://doi.org/10.1016/j.rechem.2024.101517
8. Karatas, H.; Turkmenoglu, B.; Kokbudak, Z.; Akkoc, S. Synthesis, molecular docking, and antiproliferative activity studies of bromine bearing Schiff bases. Biochemical and Biophysical Research Communications, 2025, 761, pp. 151739–151749. DOI: https://doi.org/10.1016/j.bbrc.2025.151739
9. Riaz, M.; Jan, F.; Khan, A.; Ullah, A.; Haq, H.; AlAsmari, A.F.; Alharbi, M.; Alasmari, F.; Khan, M. Unraveling the molecular structure, spectroscopic properties, and antioxidant activities of new 2,4-dinitrophenylhydrazone derivatives through a comprehensive investigation. Arabian Journal of Chemistry, 2023, 16(11), pp. 105259–105275. DOI: https://doi.org/10.1016/j.arabjc.2023.105259
10. Cao, S.; Zeng, L.-L.; Xie, J.; Wan, S.-G.; Li, D.; Zhang, H. Supramolecular helical chirality of Schiff base copper(II) complexes and their chiroptical spectroscopy. Acta Physico-Chimica Sinica, 2017, 33(12), pp. 2480–2490. DOI: https://doi.org/10.3866/PKU.WHXB201706122
11. Hari, N.; Jana, A.; Mohanta, S. Syntheses, crystal structures and ESI-MS of mononuclear-dinuclear, trinuclear and dinuclear based one-dimensional copper(II)–s block metal ion complexes derived from a 3-ethoxysalicylaldehyde–diamine ligand. Inorganica Chimica Acta, 2017, 467, pp. 11–20. DOI: https://doi.org/10.1016/j.ica.2017.07.033
12. Szymkowiak, J.; Warżajtis, B.; Rychlewska, U.; Kwit, M. One-step access to resorcinsalens-Solvent-dependent synthesis, tautomerism, self-sorting and supramolecular architectures of chiral polyimine analogues of resorcinarene. Chemistry Europe, 2018, 24(23), pp. 6041–6046. DOI: https://doi.org/10.1002/chem.201800316
13. Davis, K.J.; Assadawi, N.M.O.; Pham, S.Q.T.; Birrento, M.L.; Richardson, C.; Beck, J.L.; Willis, A.C.; Ralph, S.F. Effect of structure variations on the quadruplex DNA binding ability of nickel Schiff base complexes. Dalton Transactions, 2018, 47(38), pp. 13573–13591. DOI: https://doi.org/10.1039/C8DT02727G
14. Rigamonti, L.; Forni, A.; Cariati, E.; Malavasi, G.; Pasini, A. Solid-state nonlinear optical properties of mononuclear copper(II) complexes with chiral tridentate and tetradentate Schiff base ligands. Materials, 2019, 12(21), 3595, pp. 1–19. DOI: https://doi.org/10.3390/ma12213595
15. Cao, K.-S.; Xue, L.-W.; Liu, Q.-R. Copper(II) and nickel(II) complexes derived from isostructural bromo- and fluoro-containing bis-Schiff bases:

Syntheses, crystal structures and antimicrobial activity. Acta Chimica Slovenica, 2023, 70(4), pp. 516–523. DOI: https://doi.org/10.17344/acsi.2023.8359
16. Li, G.; Li, D.; Alshalalfeh, M.; Cheramy, J.; Zhang, H.; Xu, Y. Stereochemical properties of two Schiff-base transition metal complexes and their ligand by using multiple chiroptical spectroscopic tools and DFT calculations. Molecules, 2023, 28(6), 2571, pp. 1–22. DOI: https://doi.org/10.3390/molecules28062571
17. Hollandsworth, C.B.; Griffin, B.M.; Raymon Pruden, J.; Gerasimchuk, N.N.; Nevonen, D.E.; Nickel, R.R.; van Lierop, J.; Nemykin, V.N. Synthesis and characterization of iron(II) Schiff-base complexes of tridentate mixed amine/imine ligands with cis- and trans-1,2-diaminocyclohexane backbones. Polyhedron, 2023, 246, 116669, pp. 1–12. DOI: https://doi.org/10.1016/j.poly.2023.116669
18. Ge, C.; Cao, Z.; Feng, T.; Wu, Y.; Xiao, M.; Tang, H.; Wang, K.; Wang, L.; Li, H. Self-assembly of an unlikely occurring quadrangular tube by modulating intramolecular forces. Angewandte Chemie International Edition, 2024, 63(45), e202411401, pp. 1–6. DOI: https://doi.org/10.1002/anie.202411401
19. Balakrishnan, C.; Subha, L.; Neelakantan, M.A.; Mariappan, S.S. Synthesis, spectroscopy, X-ray crystallography, DFT calculations, DNA binding and molecular docking of a propargyl arms containing Schiff base. Spectrochimica Acta Part A, 2015, 150, pp. 671–681. DOI: https://doi.org/10.1016/j.saa.2015.06.013
20. Rubio, O.H.; Fuentes de Arriba, Á.L.; Monleón, L.M.; Sanz, F.; Simón, L.; Alcázar, V.; Morán, J.R. Bifunctional organocatalysts based on a carbazole scaffold for the synthesis of the Hajos–Wiechert and Wieland–Miescher ketones. Tetrahedron, 2015, 71(8), pp. 1297–1303. DOI: https://doi.org/10.1016/j.tet.2014.12.079
21. Guo, T.; Gou, Y.; Guo, M.; Chen, W.; Li, Y. Synthesis and solid state structures of Schiff base copper(II) and nickel(II) complexes derived from cis-1,2-diaminocyclohexane. Synthesis and Reactivity in Inorganic, Metal-Organic, and Nano-Metal Chemistry, 2015, 45(3), pp. 327–332. DOI: https://doi.org/10.1080/15533174.2013.831893
22. Liang, R.-X.; Zhang, Y.-P.; Zhang, J.-H.; Gong, Y.-N.; Huang, B.; Wang, B.-J.; Xie, S.-M.; Yuan, L.-M. Engineering thiol-ene click chemistry for the preparation of a chiral stationary phase based on a [4+6]-type homochiral porous organic cage for enantiomeric separation in normal-phase and reversed-phase high performance liquid chromatography. Journal of Chromatography A, 2023, 1711, 464444, pp. 1–10. DOI: https://doi.org/10.1016/j.chroma.2023.464444
23. Sharma, H.; Tyagi, A.; Wadawale, A.; Pandey, R. Chromogenic recognition of Cr(III) and Cu(II) using a novel Schiff base and “turn-on” fluorescent detection of CO_3^{2-} by its reduced scaffold in aqueous media. Journal of Molecular Structure, 2024, 1317, 139104, pp. 1–12. DOI: https://doi.org/10.1016/j.molstruc.2024.139104
24. Bargujar, S.; Ratnani, S.; Jain, R. Recent advances in microwave assisted synthesis of Schiff base metal complexes. Inorganic Chemistry Communications, 2024, 162, 112250, pp. 1–17. DOI: https://doi.org/10.1016/j.inoche.2024.112250
25. Haque, J.; Srivastava, V.; Chauhan, D.S.; Lgaz, H.; Quraishi, M.A. Microwave-induced synthesis of chitosan Schiff bases and their application as novel and green corrosion inhibitors: Experimental and theoretical approach. ACS Omega, 2018, 3(5), pp. 5654–5668. DOI: https://doi.org/10.1021/acsomega.8b00455
26. Al-Hiyari, B.A.; Shakya, A.K.; Naik, R.R.; Bardaweel, S. Microwave-assisted synthesis of Schiff bases of isoniazid and evaluation of their anti-proliferative and antibacterial activities. Molbank, 2021, 2021(1), M1189, pp. 1–7. DOI: https://doi.org/10.3390/M1189
27. Manjare, S.B.; Mahadik, R.K.; Manval, K.S.; More, P.P.; Dalvi, S.S. Microwave-assisted rapid and green synthesis of Schiff bases using cashew shell extract as a natural acid catalyst. ACS Omega, 2023, 8(1), pp. 473–479. DOI: https://doi.org/10.1021/acsomega.2c05187
28. Sharma, S.; Dubey, G.; Singh Sran, B.; Sharma, M.; Kaur, V.; Kaur, S.; Bharatam, P.V.; Hundal, G. Microwave-induced synthesis of pyridine based Schiff bases and their applications as efficient antimicrobial textile dyeing agents: Experimental and theoretical approach. ChemistrySelect, 2022, 7(45), e202203109, pp. 1–11. DOI: https://doi.org/10.1002/slct.202203109
29. Sarkheil, M.; Lashanizadegan, M. Schiff base ligand derived from (±)trans-1,2-cyclohexanediamine and its Cu(II), Co(II), Zn(II) and Mn(II) complexes: Synthesis, characterization, styrene oxidation and hydrolysis study of the imine bond in Cu(II) Schiff base complex. Journal of the Serbian Chemical Society, 2016, 81(4), pp. 369–382. DOI: https://doi.org/10.2298/JSC150918006S
30. Francesconi, O.; Gentili, M.; Bartoli, F.; Bencini, A.; Conti, L.; Giorgi, C.; Roelens, S. Phosphate binding by a novel Zn(II) complex featuring a trans-1,2-diaminocyclohexane ligand. Effective anion recognition in water. Organic & Biomolecular Chemistry, 2015, 13(6), pp. 1860–1868. DOI: https://doi.org/10.1039/C4OB02321H
31. Wei, Y.; Wang, S.; Zhou, S.; Feng, Z.; Guo, L.; Zhu, X.; Mu, X.; Yao, F. Aluminum alkyl complexes supported by bidentate N,N ligands: Synthesis, structure, and catalytic activity for guanylation of amines. Organometallics, 2015, 34(10), pp. 1882–1889. DOI: https://doi.org/10.1021/acs.organomet.5b00101
32. Glidewell, C.; Low, J.N.; Skakle, J.M.S.; Wardell, J.L. (1*RS*,2*RS*)-*N*,*N*′-Bis(4-nitrophenyl methylene)cyclohexane-1,2-diamine: Complex sheets built from C—H...O and C—H...π(arene)

hydrogen bonds. Acta Crystallographica Section C, 2005, 61(9), pp. o551–o554.
DOI: https://doi.org/10.1107/S0108270105024443
33. Glidewell, C.; Low, J.N.; Skakle, J.M.S.; Wardell, J.L. (1*R*,2*R*)-*N*,*N*′-Bis(4-nitrophenyl methylene)cyclohexane-1,2-diamine. Acta Crystallographica Section E: Structure Reports Online, 2005, 61, pp. o1699–o1701.
DOI: https://doi.org/10.1107/S1600536805014248
34. Matsubara, R.; Kawai, N.; Kobayashi, S. Addition of aldehyde-derived enecarbamates to *α*-oxo aldehydes. Synfacts, 2006, 9, pp. 0924–0924.
DOI: https://doi.org/10.1055/s-2006-949241
35. Cívicos, J.F.; Coimbra, J.S.M.; Costa, P.R.R. Solvent-free synthesis of salen ligands and Pd(II)– and Cu(II)–salen complexes: Their use in the oxidation of α-tetralones to α-naphthols. Synthesis, 2017, 49(17), pp. 3998–4006.
DOI: https://doi.org/10.1055/s-0036-1588446
36. Roy, K.-M. Product Subclass 4: N-nitrogen- or n-phosphorus-functionalized alkylamines (n ≥2). Enders, D.; Schaumann, E. Eds. Science of Synthesis 5: Compounds with One Saturated Carbon Heteroatom Bond. Georg Thieme Verlag: Stuttgart, 2009, pp. 615–641.
DOI: https://doi.org/10.1055/sos-SD-040-00411
37. Reeves, R.L. On the mechanism, substituent effects, and intramolecular catalysis in Schiff base hydrolysis. The Journal of Organic Chemistry, 1965, 30(9), pp. 3129–3135.
DOI: https://doi.org/10.1021/jo01020a061
38. Singh, A.; Barman, P.; Gogoi, H.P. Influence of steric and electronic effects in structure-activity relationships of Schiff base ligands: Green synthesis, characterization, DFT/TD-DFT calculations, molecular docking and biological studies. ChemistrySelect, 2022,7(48), e202204043, pp.1–13.
DOI: https://doi.org/10.1002/slct.202204043
39. Zhai, H.; Li, P.; Wang, H.; Wang, X. Temperature and steric hindrance-regulated selective synthesis of ketamine derivatives and 2-aryl-cycloketone-1-carboxamides *via* nucleophilic substitution and Favorskii rearrangement. Organic & Biomolecular Chemistry, 2025, 23(11), pp. 2704–2711.
DOI: https://doi.org/10.1039/D4OB02039A
40. Furtado, L.B.; Nascimento, R.C.; Henrique, F.J.F.S.; Guimarães, M.J.O.C.; Rocha, J.C.; Ponciano, J.A.C.; Seidl, P.R. Effects of temperature, concentration and synergism on green Schiff bases synthesized from vanillin in applications as corrosion inhibitors for carbon steel in well stimulation. Journal of Petroleum Science and Engineering, 2022, 213, 110401, pp. 1–13.
DOI: https://doi.org/10.1016/j.petrol.2022.110401
41. Ledeţi, I.; Alexa, A.; Bercean, V.; Vlase, G.; Vlase, T.; Şuta, L.-M.; Fuliaş, A. Synthesis and degradation of Schiff bases containing heterocyclic pharmacophore. International Journal of Molecular Sciences, 2015, 16(1), pp. 1711–1727.
DOI: https://doi.org/10.3390/ijms16011711
42. El Hamdaoui, L.; El Marouani, M.; El Bouchti, M.; Kifani-Sahban, F.; El Moussaouiti, M. Thermal stability, kinetic degradation and lifetime prediction of chitosan Schiff bases derived from aromatic aldehydes. ChemistrySelect, 2021, 6(3), pp. 306–317.
DOI: https://doi.org/10.1002/slct.202004071
43. Ahmed, D.S.; Kadhom, M.; Hadi, A.G.; Bufaroosha, M.; Salih, N.; Al-Dahhan, W.H.; Yousif, E. Tetra Schiff bases as polyvinyl chloride thermal stabilizers. Chemistry, 2021, 3(1), pp. 288–295.
DOI: https://doi.org/10.3390/chemistry3010021
44. Alamri, A.A.; Borik, R.M.A.; El-Wahab, A.H.F.A.; Mohamed, H.M.; Ismail, K.S.; El-Aassar, M.R.; Al-Dies, A.-A.M.; El-Agrody, A.M. Synthesis of Schiff bases based on chitosan, thermal stability and evaluation of antimicrobial and antitumor activities. Scientific Reports, 2025, 15(1), 892, pp. 1–14.
DOI: https://doi.org/10.1038/s41598-024-73610-6
45. Hafidh, S.H.; Muslim, R.F.; Awad, M.A. Characterization and biological effectiveness of synthesized complexes of palladium (II) from imine compounds. Egyptian Journal of Chemistry, 2022, 65(1), pp. 385–396. DOI: https://doi.org/10.21608/ejchem.2021.79085.3876
46. Aazza, M.; Mounir, C.; Ahlafi, H.; Bouymajane, A.; Cacciola, F. Performance of first derivative UV/Visible spectra for kinetic and isothermal study of simultaneous adsorption of o-nitrophenol and *p*-nitrophenol onto Al_2O_3 and $HDTMA^+/Al_2O_3$ composite. Journal of Molecular Liquids, 2023, 383, 122139, pp. 1–11.
DOI: https://doi.org/10.1016/j.molliq.2023.122139
47. Monteiro-de-Castro, G.; Borges Jr., I. A Hammett's analysis of the substituent effect in functionalized diketopyrrolopyrrole (DPP) systems: optoelectronic properties and intramolecular charge transfer effects. Journal of Computational Chemistry, 2023, 44(29), pp. 2256–2273.
DOI: https://doi.org/10.1002/jcc.27195
48. Sobczak, P.; Sierański, T.; Świątkowski, M.; Trzęsowska-Kruszyńska, A.; Kolińska, J. Unraveling the structure–property relationships in fluorescent phenylhydrazones: the role of substituents and molecular interactions. RSC Advances, 2025, 15(3), pp. 1514–1526.
DOI: https://doi.org/10.1039/D4RA07856J
49. Yang, Y.; Luo, X.; Ma, F.; Li, Y. Substituent effect on ESIPT mechanisms and photophysical properties of HBT derivatives. Spectrochimica Acta Part A, 2021, 250, 119375, pp. 1–11.
DOI: https://doi.org/10.1016/j.saa.2020.119375